

Article

Prediction of the Roughness Reduction in Centrifugal Disc Finishing of Additive Manufactured Parts Based on Discrete Element Method

Marco Kopp ^{1,*} and Eckart Uhlmann ^{1,2}

¹ Institute for Machine Tools and Factory Management (IWF), Technische Universität Berlin, Pascalstr. 8-9, 10587 Berlin, Germany

² Fraunhofer Institute for Production Systems and Design Technology IPK, Pascalstr. 8-9, 10587 Berlin, Germany

* Correspondence: kopp@iwf.tu-berlin.de; Tel.: +49-30-314-23624

Abstract: One major drawback of additive manufacturing is the poor surface quality of parts, which negatively affects mechanical and tribological properties. Therefore, a surface finishing is necessary in most cases. Due to a high material removal rate, centrifugal disc finishing is a promising mass finishing operation for an effective surface finishing of additive manufactured parts. However, due to machining the workpieces in a freely movable manner, the process is hardly controllable, and the process design is often based on time-consuming and cost-intensive trial-and-error approaches. Especially when it comes to the machining of complex-shaped workpieces, finishing results are barely predictable. Therefore, the aim of this study is to set up a numerical simulation of the centrifugal disc finishing based on the Discrete Element Method (DEM) to predict finishing results. A procedure to determine the required DEM input parameters is presented and the simulation was validated using a freely movable force sensor. The results of the finishing experiments with additive manufactured workpieces made of Ti-6Al-4V were correlated with the simulated results. The derived correlation was used to predict local differences in the roughness reduction, which occurred when finishing workpieces with a limited accessibility to the surface. As a result, it is concluded that the complex relationship between the type of media, the accessibility to the surface, and the achievable finishing results can be modeled using the DEM.

Keywords: mass finishing; centrifugal disc finishing; additive manufactured workpieces; discrete element method; roughness reduction; modeling



Citation: Kopp, M.; Uhlmann, E. Prediction of the Roughness Reduction in Centrifugal Disc Finishing of Additive Manufactured Parts Based on Discrete Element Method. *Machines* **2022**, *10*, 1151. <https://doi.org/10.3390/machines10121151>

Academic Editor: Angelos P. Markopoulos

Received: 14 November 2022

Accepted: 30 November 2022

Published: 1 December 2022

Publisher's Note: MDPI stays neutral with regard to jurisdictional claims in published maps and institutional affiliations.



Copyright: © 2022 by the authors. Licensee MDPI, Basel, Switzerland. This article is an open access article distributed under the terms and conditions of the Creative Commons Attribution (CC BY) license (<https://creativecommons.org/licenses/by/4.0/>).

1. Introduction

Centrifugal disc finishing is a mass finishing operation, in which free movable workpieces are machined in a bulk of abrasive media. The relative movement between the media and the workpieces is initiated by a rotating disc at the bottom of a stationary finishing bowl. The advantage of centrifugal disc finishing is a high material removal rate compared with other mass finishing processes such as the widely used vibratory finishing [1]. The high achievable material removal rate is especially advantageous for the finishing of additive manufactured parts as it enables an effective reduction of the high as-built surface roughness [2] and thus an increase in the fatigue life [3–5] and wear resistance of parts [6,7]. However, as the workpieces in centrifugal disc finishing are machined in a freely movable manner, the process is less controllable compared with mass finishing operations with a fixed workpiece such as drag finishing, in which a defined positioning of the workpiece within the bulk of moving media and thus a selective machining is possible [8–10]. Consequently, in order to enable the centrifugal disc finishing as an effective finishing operation for additive manufactured parts, it is necessary to make the process predictable and replace the commonly used trial-and-error approach for process design. Especially the finishing of

complex-shaped workpieces, which usually occur with additive manufacturing, is a challenge, as the accessibility of the media to the workpiece surface is a considerable influential factor regarding the finishing performance [11]. Eulitz [11] proposes a process simulation based on the Discrete Element Method (DEM) to analyze the complex relationship between the type of media, the accessibility of the workpiece surface, and the local machining intensity on the workpiece. The DEM is a numerical method to calculate the mechanical behavior of an assembly of particles [12]. The DEM is based on an alternating application of force–displacement laws to calculate the forces acting on the particles and Newton’s second law of motion and motion integration to determine the velocities and the positions of the particles [12], Figure 1.

F_p :	total force on particle	F_c :	contact force
g :	gravitational acceleration	$F_{c,n}/F_{c,t}$:	contact normal/tangential force
m_p :	mass of particle	s_n/s_t :	normal/tangential displacement
t_{sim} :	simulation time	\dot{s}_n/\dot{s}_t :	derivative of normal/tangential displacement
Δt_{sim} :	timestep of simulation	k_n/k_t :	normal/tangential stiffness coefficient
x_p :	position of particle	μ_{stat} :	coefficient of static friction
\ddot{x}_p :	acceleration of particle		

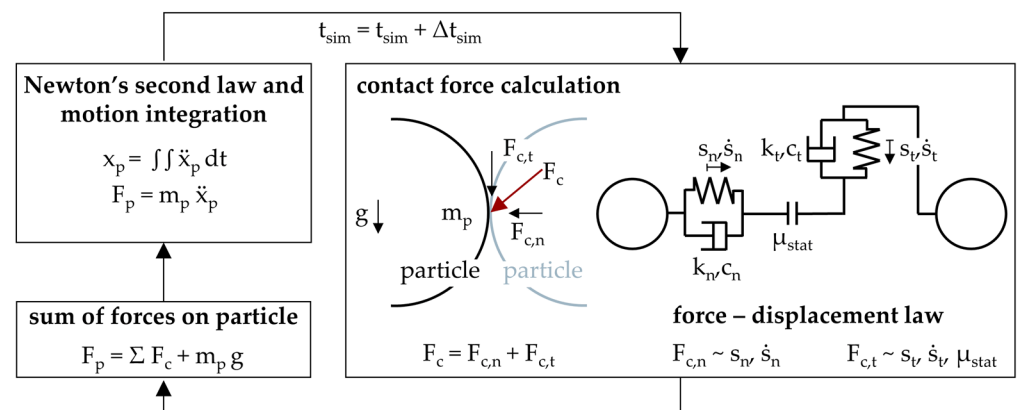


Figure 1. DEM calculation cycle.

The DEM was used in several studies to analyze mass finishing operations. In the first approach, forces acting on a workpiece in drag finishing were modeled with a deviation of 23% [13]. Naeini and Spelt [14,15] modeled the motion of spherical steel media in a vibratory tube. The media velocity was simulated with a deviation from measurements of less than 10% [14]. In a following study, it was found that the media velocity increases with the amplitude of the tube vibration as well as with the magnitude of the media–media friction and the media–wall friction [15]. Hashemnia and Spelt [16,17] simulated the media velocity as well as the impact velocity of the media with a deviation of less than 30% and 19% from measurements, respectively. In following studies, the model was used to analyze the influence of the vibratory excitation and the friction between the media and the tube wall on the media motion [18–21]. It was found that the media velocity was mostly affected by the vertical amplitude of the tube vibration [18]. The forces between the media and the wall increased with an increasing vibration frequency [19]. Contrary to Naeini and Spelt [15], the media–wall friction was found to have no influence on the media velocity [18]. Kang et al. [22] investigated the motion of spherical media in a vibratory finishing machine using the DEM. It was found that contact parameters such as the contact stiffness and the contact damping have a strong influence on the simulated media motion. Wang et al. [23] correlated the finishing results of workpieces fixed in varying positions to the wall of a vibratory machine with simulated forces obtained by DEM modeling. The highest forces were observed at the bottom of the machine, which is consistent with results from finishing experiments [23]. Makiuchi et al. [24] calculated contact forces and relative velocities between the media and the workpieces in vibratory finishing using the DEM.

The simulated results were used to predict the material removal and the surface roughness based on Hertzian contact theory and Preston's law. The predictions differed from the experimental results by 12% on average. Salvatore et al. [25] calculated the sliding velocity and the contact forces of the media on the surface of a workpiece in drag finishing using the DEM. However, due to a different wear mechanism on the workpiece depending on the impact angle of the media, roughness reduction could not be predicted from the simulated results. Zanger et al. [8] qualitatively predicted the influence of process parameters in drag finishing by correlating contact forces and tangential contact velocities obtained by DEM simulations with the material removal rate and residual stresses of workpieces. As shown in previous studies, the DEM can also be performed using aspherical media [26–29]. In robot-guided drag finishing, contact characteristics of spherical and prismatic media such as the contact force, the contact frequency, and the contact duration were determined in experiments and could be reflected by DEM simulations [26]. In robot-guided centrifugal disc finishing, a material removal model based on DEM simulations was derived, predicting the material removal rate of prismatic media with an average error of 13% [27]. Furthermore, the DEM was used to model the influence of media wear on finishing results in centrifugal disc finishing [28]. Recent developments in the DEM also allow the modeling of lubrication conditions as shown in a previous study dealing with drag finishing using cone-shaped media [29].

It should be mentioned that there are also modeling approaches where the bulk of media is treated as a continuous material, as for example in computational fluid dynamics [9,10,30–34]. However, these approaches do not allow the modeling of individual contacts between the media and the workpiece, which is of particular importance in mass finishing processes [11].

Although there are several studies dealing with DEM simulations of mass finishing, the determination of the contact parameters required for the DEM is often treated as a black box when setting up the model. In some studies, a comprehensible determination of contact parameters of steel media is presented [14,17]. However, these contact parameters cannot be used in the modeling of industrially relevant processes, as in most cases ceramic media is used. Other studies simplify the procedure of the contact parameter determination by assuming that the walls of the finishing machine are made of steel [11,13,26–28], which barely reflects industrial applications where polyurethane coating is used to prevent wear of the walls. In most studies, the used contact parameters or the methodology of their determination are not completely presented [8,22,24,25,29].

Against this background, the aim of this study is to present a comprehensible procedure for the determination of contact parameters for ceramic media of different shapes. The final DEM simulation setup was validated using force measurements obtained by a freely movable force sensor [35]. Based on the results from DEM simulations, a prediction model was derived, which enabled the prediction of the local roughness reduction of additive manufactured workpieces in centrifugal disc finishing.

2. Materials and Methods

2.1. Machining Setup

The investigations were carried out in a centrifugal disc finishing machine MPA 07.1 A2 by Rösler Oberflächentechnik GmbH, Untermerzbach, Germany, Figure 2a. Three types of ceramic-bonded media were used, which were made of the same material and differed in size and shape, Figure 2b. The three media types were spherical RS 11 G, cylindrical RS 07/15 ZS, and prismatic RS 10/15 S by Rösler Oberflächentechnik GmbH. Each experiment was conducted with a total media mass of $m_{m,tot} = 30$ kg and a circulated process rinsing with a volume flow of $\dot{V}_c = 0.5$ L min⁻¹ of a 1% solution of a universal cleaning agent compound with corrosion protection of the type ZF 113 by Rösler Oberflächentechnik GmbH.

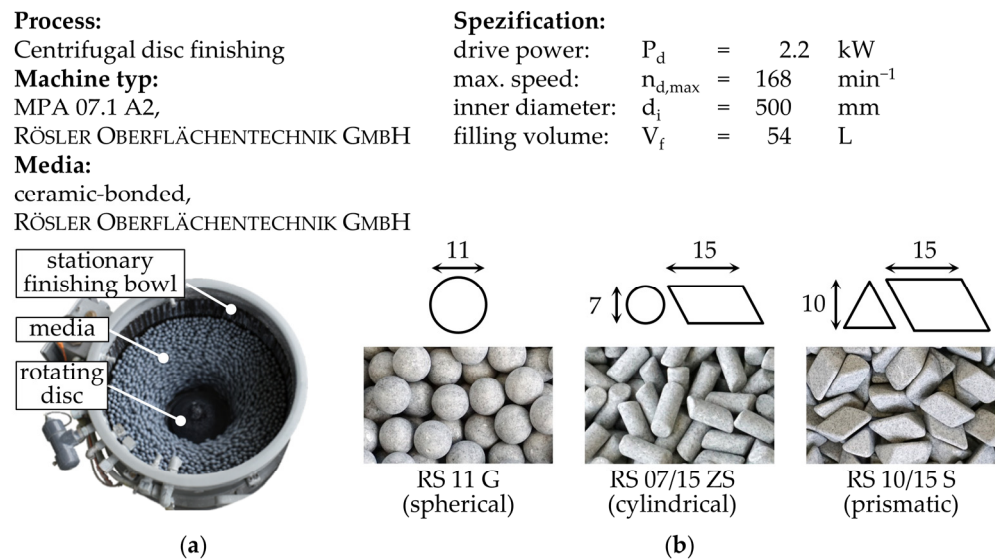


Figure 2. Machining setup: (a) finishing machine; (b) finishing media.

2.2. Force Measurements

For measuring the normal forces exerted by the media on the workpiece, a self-developed, wireless measuring system based on strain gauges was used, Figure 3. The normal force resulting from media touching the contact body was transmitted to a load cell of the type KM 10 25 N by ME-Meßsysteme GmbH, Henningsdorf, Germany. The output voltage from the load cell was amplified by an amplifier of the type AD620A by Analog Devices Inc., Norwood, MA, USA, and was fed into a Teensy 4.1 microcontroller by PJRC, Sherwood, OH, USA, where it was digitized with a resolution of 10 bits and a sampling rate of 20 kHz and was written to an SD card. The power supply was provided by a 3.6 V lithium-polymer accumulator and a voltage converter of the type MiniBoost 5 V by Adafruit Industries LLC, New York, NY, USA. The communication with the measuring system was realized using a Bluetooth module of the type HC-05. All components were mounted on an inner casing made of polylactide manufactured by fused deposition modeling. The outer casing as well as the contact body consisted of stainless steel 1.4301. To ensure a realistic mass comparable to an equal-sized workpiece, lead weights were integrated in the measuring system. The total mass of the measuring system was 562 g. The contact area of the contact body had a diameter of 10 mm. Measurements with a covered contact body showed that the oscillation of the contact body resulted in normal forces of up to 0.3 N. To account for this uncertainty in the measurements, a normal force threshold of $F_{n,th} = 0.3$ N was defined, below which a normal force was not considered as being exerted by the media. Each measurement took 30 s and was carried out six times.

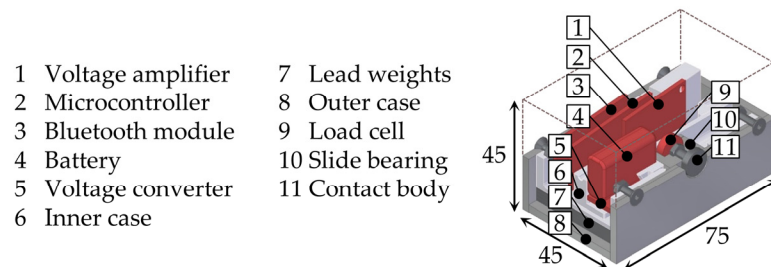


Figure 3. Force measurement device.

2.3. Finishing Experiments

Finishing experiments were carried out with workpieces made of Ti-6Al-4V manufactured by laser powder bed fusion. All workpieces were manufactured in a single building

job, Figure 4a, and then wire-eroded into cubes with an edge length of 20 mm. Based on these cubes, two workpiece variants were realized by mounting different adapters made of stainless steel 1.4301 on the cubes, Figure 4b. Workpiece variant A was characterized by a freely accessible surface to be machined, whereas the surface of the workpiece variant B was shielded by the adapters and thus had a limited accessibility. Both workpiece variants were designed to have the same mass of 105 g.

Manufacturing process:	Material:	Process parameters:
Laser powder bed fusion	Ti-6Al-4V	Layer thickness: 30 μm
Machine Type:	Grain size: 15–45 μm	Laser Power: 400 W
Renishaw RenAM 500Q HT		Exposure time: 40 μs

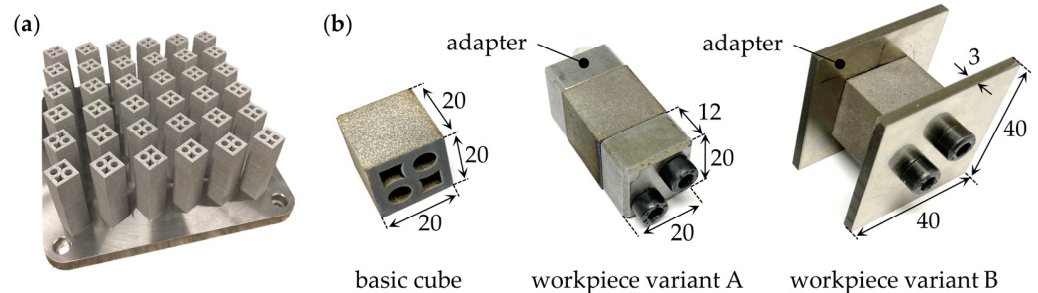


Figure 4. Workpieces of finishing experiments: (a) as built; (b) eroded basic cube and workpiece variants.

The surface roughness was measured with a skid system of the type SurfTest SJ-210 by Mitutoyo Deutschland GmbH, Neuss, Germany, according to DIN EN ISO 4287 [36] and DIN EN ISO 4288 [37]. All finishing experiments were carried out two times. Each time, one of each of the workpiece variants was machined simultaneously.

2.4. Process Modeling

2.4.1. Simulation Setup

The process was simulated based on the DEM using the software Rocky DEM 22.2.0 by Engineering Simulation and Scientific Software Inc. (Esss), Florianópolis, Brazil. To set up the simulation, STL models of all components of the experiments, i.e., the finishing bowl and the rotating disc, the media, and the workpieces, were created, Figure 5. As the inner walls of the finishing machine were coated with polyurethane, preventing wear, polyurethane was the assigned material of the finishing machine in the simulations. All types of media were of the same ceramic material. Thus, it was assumed that the material parameters and the contact parameters were the same for all media types, which is of particular importance as not all experiments of the parameter determination can be carried out with all types of media due to their shapes. The simulations of the force measurements were carried out with a simplified geometrical model of the force sensor, which only consisted of a solid cubic body of the same dimensions as the real force sensor. As the real force sensor consisted of an outer casing made of stainless steel 1.4301, the material assigned to the simplified model of the force sensor was steel. However, the density ρ of the force sensor was adjusted in the simulations to match the mass of the real force sensor, as real force sensor did not consist of solid steel.

The simulations of the finishing experiments were carried out with simplified geometrical models of the workpiece variants A and B. Although the workpiece variants consisted of 1.4301 and Ti-6Al-4V, for simplification purposes, only steel was the assigned material in the simulations. However, to match the masses of the workpiece variants A and B, the density ρ was adjusted in the simulations. A summary of all the materials assigned to each component as well as the material parameters required for the simulation are listed in Table 1.

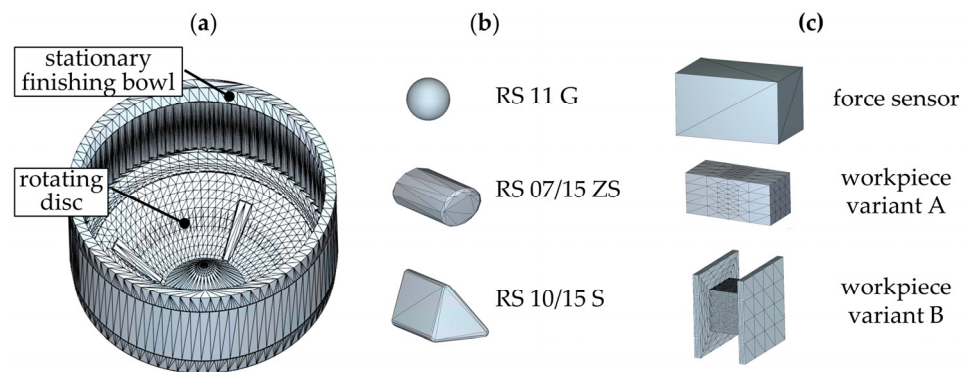


Figure 5. STL models of the simulation components (not true to scale): (a) finishing machine; (b) media; (c) workpieces.

Table 1. Material parameters of the simulation components.

Component of Simulation	Material	Density ρ	Young's Modulus E	Poisson Ratio ν
-	-	g cm^{-3}	GPa	-
media	ceramic	2.52 *	77 **	0.19 **
workpiece	steel	force sensor: 3.61 workpiece variant A/B: 5.93	210	0.3
finishing machine	polyurethane	1.25	0.1	0.45

* manufacturer datasheet; ** Uhlmann et al. [13].

2.4.2. Contact Force and Timestep Calculation

Contact forces were calculated with the force–displacement laws derived by Cundall and Strack [12]. The normal component of the contact force $F_{c,n}$ involves a linear elastic term including the normal stiffness coefficient k_n and the normal displacement s_n as well as a viscous damping term including the damping coefficient c_n and the time derivative of the normal displacement \dot{s}_n , Equation (1).

$$F_{c,n} = k_n s_n + c_n \dot{s}_n \quad (1)$$

The normal stiffness coefficient k_n is directly related to the Young's modulus E of the two components in contact. As common practice in DEM simulations, the damping coefficient c_n is based on the energy dissipation due to an inelastic collision, which can be expressed by the coefficient of restitution e of the components in contact [38,39]. As a simplification of the force–displacement law derived by Cundall and Strack [12], only a linear elastic term including the tangential stiffness coefficient k_t and the tangential displacement s_t is used to calculate the tangential component of the contact force $F_{c,t}$, Equation (2).

$$F_{c,t} = k_t s_t \quad (2)$$

For simplification purposes, the tangential stiffness coefficient k_t is set equal to the normal stiffness coefficient k_n . The tangential contact force $F_{c,t}$ is limited by the maximum tangential contact force $F_{c,t,max}$ defined by the Coulomb friction law considering the coefficient of static friction μ_{stat} of the components in contact [12], Equation (3).

$$F_{c,t,max} = \mu_{stat} F_{c,n} \quad (3)$$

As proposed by Tsuji et al. [40], the timestep of the simulation Δt_{sim} was chosen based on the oscillation period of an equivalent spring–mass system considering the equivalent mass m^* as well as the normal stiffness coefficient k_n of the components in contact [40].

As simulations with aspherical media were carried out in this study, a twentieth of the oscillation period of an equivalent spring–mass system was used as a timestep to ensure numerical stability, Equation (4).

$$\Delta t_{\text{sim}} = 2\pi\sqrt{m^*/k_n} / 20 \quad (4)$$

2.4.3. Contact Parameter Determination

For each possible contact combination, i.e., media–media contact, media–workpiece contact, and media–finishing machine contact, the coefficient of static friction μ_{stat} and the coefficient of restitution e must be determined. This was done using a series of experiments suggested by González-Montellano et al. [41]. The coefficient of static friction of the media–media contact $\mu_{\text{stat,m-m}}$, the media–workpiece contact $\mu_{\text{stat,m-w}}$, and the media–finishing machine contact $\mu_{\text{stat,m-fm}}$ were determined using an inclined plane, Figure 6a. Three samples of each component’s material, i.e., steel, polyurethane, and pieces of media were glued on an upper and a lower sample tray in a triangular arrangement. The lower sample tray was fixed on the inclinable platform. With the inclinable platform in horizontal position, the upper sample tray was placed on the lower sample tray so that the samples were on top of each other. To account for the varying load collectives, different loading masses were placed on the upper sample tray. The inclinable plane was raised using a 12 V direct current gear motor with a constant inclination speed of $\omega_i = 0.7 \text{ s}^{-1}$ until the upper sample tray began to slide. At the moment of sliding, the raising mechanism was stopped and the inclination angle α_i was measured. The related coefficient of static friction μ_{stat} of the contact combination can be calculated as follows [41]:

$$\mu_{\text{stat}} = \tan(\alpha_i) \quad (5)$$

As inclined plane experiments should preferably be carried out with the materials under test having a plane surface contact, only the prismatic media RS 10/15 S was used in the experiments. For this reason, the media were glued together as shown exemplarily for the media–media contact in the detail view of Figure 6a. Experiments with each contact combination were carried out ten times with different samples of the components.

The coefficient of restitution of the media–finishing machine contact $e_{\text{m-fm}}$ and the media–workpiece contact $e_{\text{m-w}}$ was determined by drop tests [41], Figure 6b. In this test, samples of the spherical media RS 11 G are dropped from a defined height onto a flat surface made of steel and polyurethane, which represent the workpiece and the finishing machine, respectively. Assuming that the media only has a vertical velocity component before and after the contact, the coefficient of restitution e can be calculated using the height before contact h_0 and the height after contact h_1 [41]:

$$e = \sqrt{\tan(h_1/h_0)} \quad (6)$$

The coefficient of restitution of the media–media contact $e_{\text{m-m}}$ was determined using a double pendulum [41], Figure 6c. Samples of the spherical media RS 11 G were glued to nylon strings, which were fixed to a horizontal bar. One piece of media—sample 1—was displaced laterally to a defined height. After releasing sample 1, it collided with sample 2. The coefficient of restitution e can be calculated using the height before contact h_0 and the height after contact of sample 1 and sample 2, i.e., h_1 and h_2 [41]:

$$e = (\sqrt{h_2} - \sqrt{h_1}) / \sqrt{h_0} \quad (7)$$

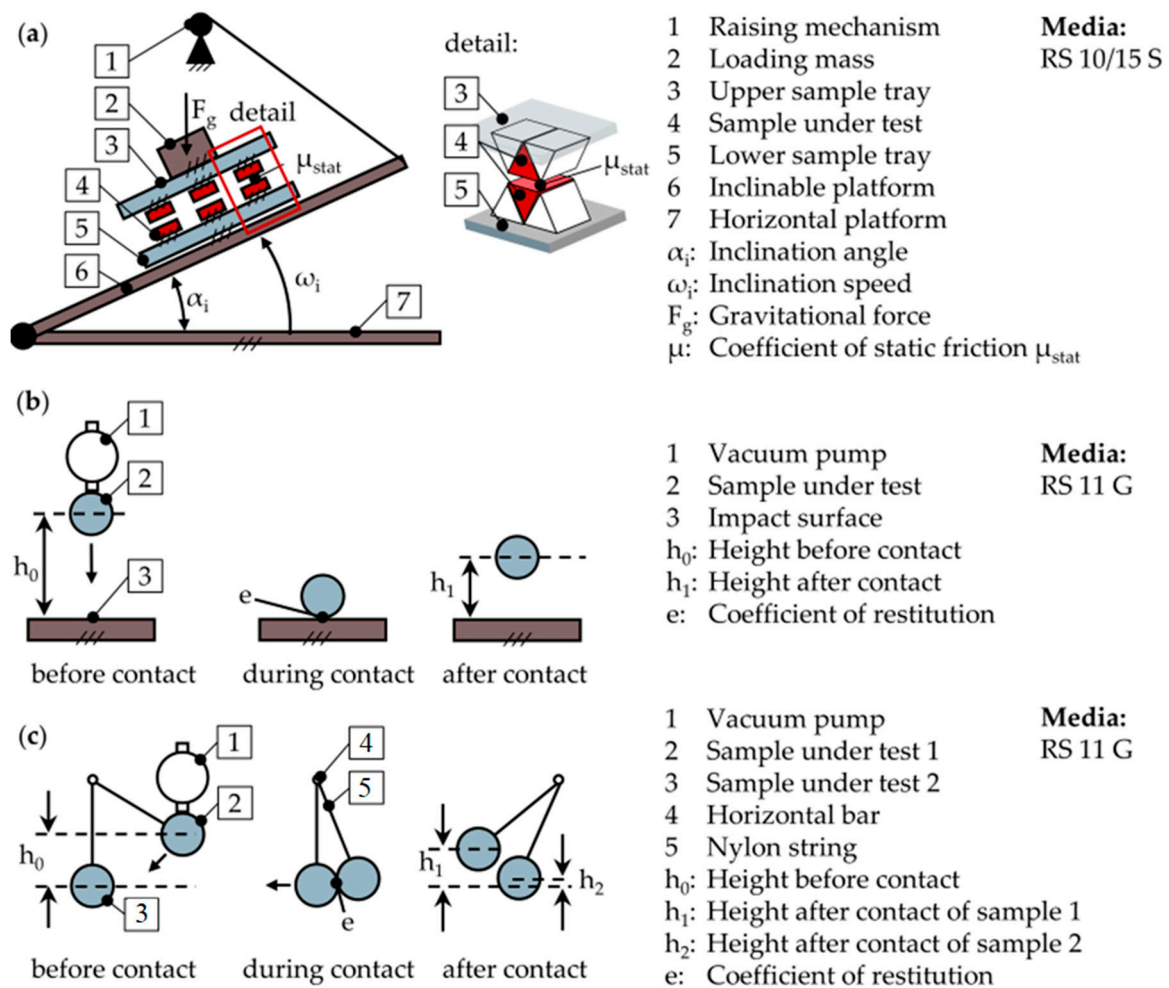


Figure 6. Experiments of DEM parameter determination: (a) inclined plane; (b) drop test; (c) double pendulum.

The heights in the drop test and the double pendulum were determined using a camera running at 120 fps. The height before contact h_0 varied in both experiments. At each height, tests were carried out ten times with different samples.

3. Results

3.1. Contact Parameters

The results of the inclined plane experiment showed that the gravitational force F_g exerted on the samples had a negligible influence on the coefficient of static friction μ_{stat} for all contact combinations, Figure 7a. Thus, for each contact combination, the mean value of the coefficient of static friction μ_{stat} was calculated over the varied gravitational force F_g . The determined coefficients of static friction of the media–media contact, the media–workpiece contact, and the media–finishing machine contact were $\mu_{stat,m-m} = 0.41$, $\mu_{stat,m-w} = 0.27$, and $\mu_{stat,m-fm} = 0.93$, respectively. The high value of the coefficients of static friction $\mu_{stat,m-fm}$ of the media–finishing machine contact was a result of abrasive grains penetrating the soft surface of the polyurethane sample. The results of the drop tests showed constant coefficients of restitution e over the investigated heights before contact h_0 for both contact combinations, Figure 7b. The coefficients of restitution were determined as $e_{m-w} = 0.95$ for the media–workpiece contact and $e_{m-fm} = 0.76$ for the media–finishing machine contact. Although the coefficient of restitution for the media–media contact e_{m-m} slightly increased with increasing heights before contact h_0 , its mean value of $e_{m-m} = 0.72$ was considered as an input parameter for the simulation.

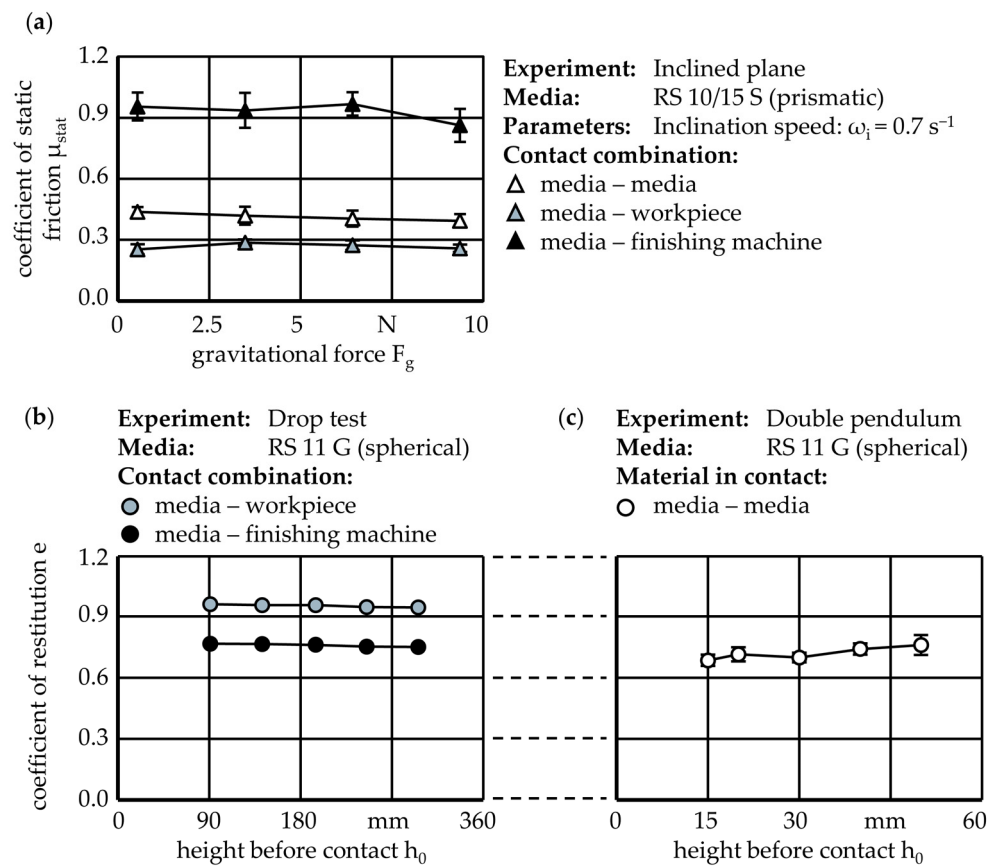


Figure 7. Results of DEM parameter determination: (a) inclined plane; (b) drop test; (c) double pendulum.

To reduce the computational time of the simulations t_{comp} , a reduction of the contact stiffness was performed by multiplying the normal stiffness coefficient k_n with a stiffness factor of $f_k < 1$ [42]. Reducing the stiffness factor f_k led to a decrease in contact normal forces $F_{c,n}$ for all rotational speeds n_d and media types, Figure 8a. A further reduction of the stiffness factor to less than $f_k = 1 \cdot 10^{-3}$ led to an unstable simulation behavior; thus, a stiffness factor of $f_k = 1 \cdot 10^{-3}$ was identified as a limiting reduction of the normal stiffness coefficient k_n . Reducing the normal stiffness coefficient k_n in this order of magnitude reduced the absolute values of the contact normal forces $F_{c,n}$ by 94% on average. However, the computational time t_{comp} was reduced by 90% on average by using a stiffness factor of $f_k = 1 \cdot 10^{-3}$, Figure 8a. For the reason of comparison, the results from the simulations with a stiffness factor of $f_k = 1 \cdot 10^0$ —meaning that there was no stiffness reduction—and the results from the simulations with a stiffness factor of $f_k = 1 \cdot 10^{-3}$, the contact normal forces $F_{c,n}$ were normalized, Figure 8b. For both stiffness factors f_k , a positive correlation between the rotational speed n_d and the resulting contact forces can be found. Furthermore, for both stiffness factors f_k , the highest contact forces occurred for the prismatic media type RS 10/15 S, followed by the spherical media type RS 11 G and the cylindrical media type RS 07/15 SZ. Accordingly, the contact forces seemed to correlate with the size of the media.

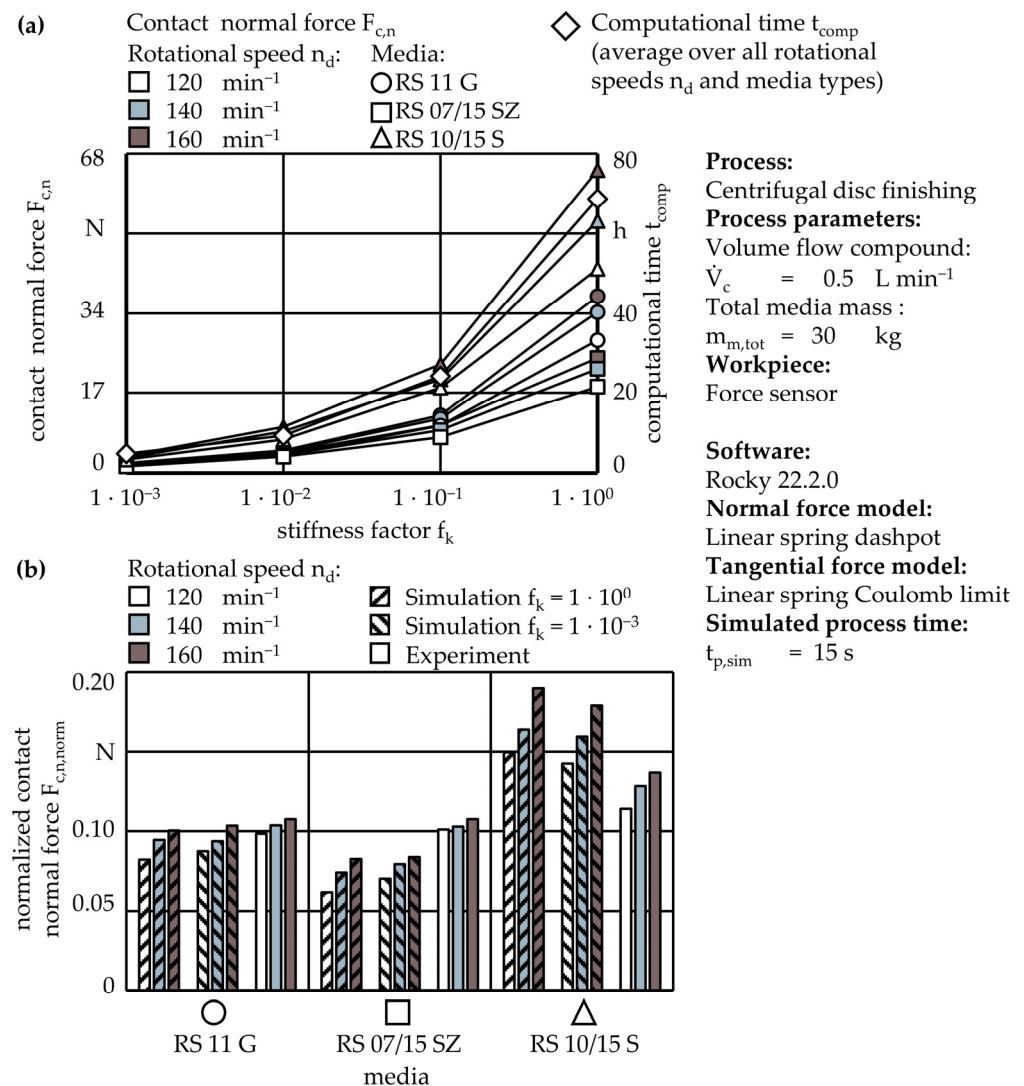


Figure 8. Simulation of contact forces: (a) influence of stiffness reduction on contact forces; (b) comparison of simulated and experimental contact forces.

3.2. Validation

As found out in the previous section, reducing the contact stiffness led to a downscaling of the contact forces while the effects of the influential factors remained observable and the computational time t_{comp} was reduced. Consequently, further simulations were carried out with a stiffness factor of $f_k = 1 \cdot 10^{-3}$. Only the results of this simulation configuration were compared to the normalized contact normal forces $F_{c,n, norm}$ obtained by force measurement experiments, Figure 8b. A detailed description and analysis of the force measurement experiments is presented in a previous study [35]. For the spherical media type RS 11 G, the deviation of the simulated results from the experimental results was on average 8%. Increasing the rotational speed from $n_d = 120 \text{ min}^{-1}$ to $n_d = 160 \text{ min}^{-1}$ for this media type led to an increase in the contact forces by 9% in the experiments, while the simulated contact forces were increased by 18%. Thus, the effect of the rotational speed n_d was overestimated in the simulations. This also applied to the cylindrical media type RS 07/15 SZ, where an increase in the rotational speed n_d led to an increase in the contact forces by 6% in the experiments and 19% in the simulations. Furthermore, the contact forces for the cylindrical media type RS 07/15 SZ were on average 25% lower than in the experiments. This might be attributed to the fact that in the experiments, the contact forces were detected with a contact body that could be in contact with several pieces of cylindrical media simultaneously. These

simultaneous contacts could not be evaluated separately from each other, so they were detected as a single contact, which led to a bias in the measured contact forces. This bias did not exist in the simulation as it allowed for a separate evaluation of all the individual contacts on the entire surface of the force sensor. The experimental results confirmed that for the prismatic media type RS 10/15 S, the highest contact forces occurred. However, the simulated results were on average 26% higher than in the experiments. Again, the influence of the rotational speed n_d was overestimated in the simulations, as increasing the rotational speed from $n_d = 120 \text{ min}^{-1}$ to $n_d = 160 \text{ min}^{-1}$ led to an increase in the contact forces by 20% in the experiments while the simulated contact forces were increased by 25%. Overall, the simulated contact forces had an average deviation of 20% from experimental results.

3.3. Correlation of Finishing and Simulated Results

To correlate the finishing results with simulated characteristics, finishing experiments were carried out with the workpiece variant A. The surface roughness, which was achieved after a processing time of $t_p = 120 \text{ min}$, was influenced by both the type of media as well as the rotational speed n_d , Figure 9a. For all media types, the achievable surface roughness decreased with an increasing rotational speed n_d . This can be explained with increased contact forces, Figure 8b, as well as increased contact frequencies f_c between the media and the workpiece when increasing the rotational speed n_d [35]. Both increased contact forces as well as increased frequencies f_c led to a high material removal rate, resulting in effectively reducing the high initial surface roughness Ra_0 . For all rotational speeds n_d , the smallest surface roughness could be achieved with the prismatic media type RS 10/15 S, followed by the cylindrical media type RS 07/15 SZ and the spherical media type RS 11 G. It should be mentioned that this does not reflect the order of the contact forces observed for the media types, Figure 8b. However, the order of the achievable surface roughness was related to the material removal rate, which is influenced by the shape of the media [11,27]. As the prismatic media type contains several plane surfaces, machining is conducted by long-term sliding with a large area being in contact with the workpiece, which leads to a high material removal rate caused by abrasion [11,35]. Contrarily, the spherical media type is of a pure convex shape, which results only in punctual short-term impacts with the workpiece, leading to a low material removal rate [11,35]. The material removal rate of the cylindrical media type is between that of the prismatic and spherical media types, as the cylindrical shape leads to line contacts with the workpiece, resulting in a contact area larger than punctual contacts but smaller than surface contacts [11].

DEM simulations of the finishing experiments were carried out with the simplified geometrical model of the workpiece variant A. Only the area on the workpiece surface corresponding to the roughness measurements of the finishing experiments was evaluated. As the reduction of the surface roughness was not only influenced by the contact normal force $F_{n,c}$, Figures 8b and 9a, the prediction of the finishing results only by considering the simulated contact normal force $F_{n,c}$ would be insufficient. The average contact intensity I_c was found to correlate with the relative reduction of the roughness ΔRa , Figure 9b, reflecting both the effect of the rotational speed n_d as well as the media type. The contact intensity I_c was calculated by adding up the contact works W_c transferred by all contacts within a given time interval Δt_c to a unit area A_c :

$$I_c = \Sigma W_c / (\Delta t_c A_c) \quad (8)$$

The contact work W_c is defined as the integral of the contact normal force $F_{c,n}$ over the normal displacement s_n of a contact:

$$W_c = \int F_{c,n} ds_n \quad (9)$$

Under the assumption that a contact intensity of $I_c = 0 \text{ Wm}^{-2}$ would not result in any reduction of the surface roughness ΔRa , an empirical fitting with a power law approach leads to a best fit of:

$$\Delta Ra = 61.315 I_c^{0.153} \quad (10)$$

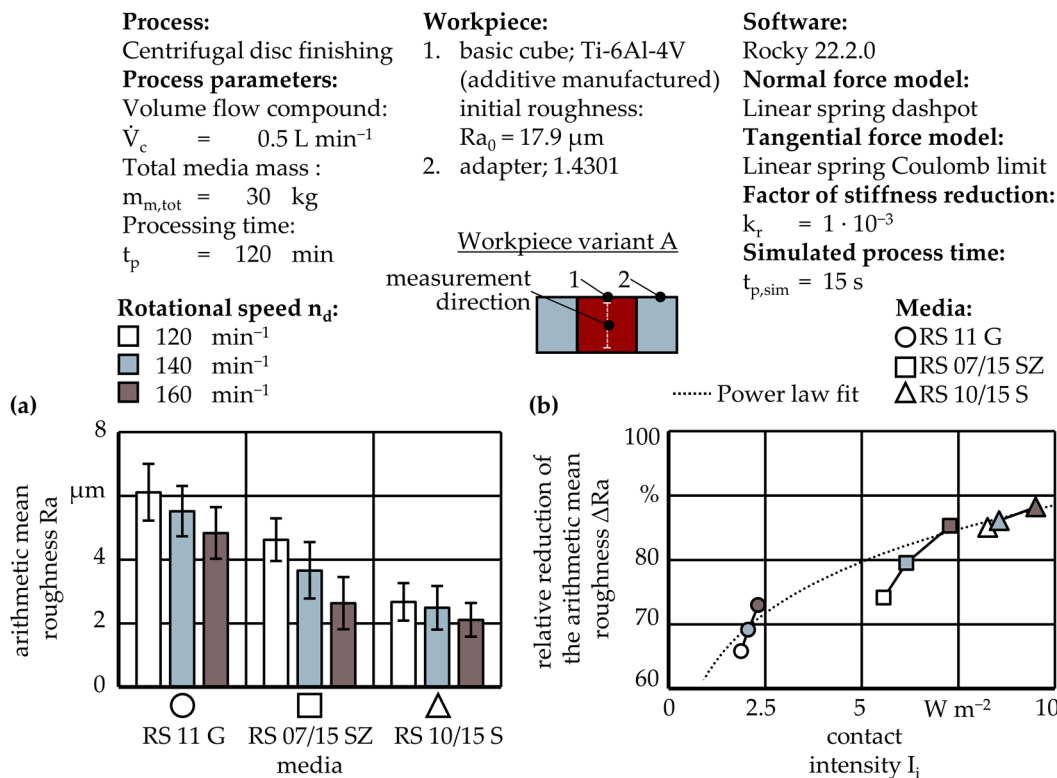


Figure 9. Workpiece variant A: (a) results of finishing experiments; (b) correlation between experimental and simulated results.

3.4. Prediction of Finishing Results

To test if the derived prediction model, Equation (10), is valid for workpieces with limited accessibility to the surface, finishing experiments with the workpiece variant B were carried out. As expected, the limited surface accessibility led to local differences in roughness reductions ΔRa , which depend on the type of media, Figure 10a. For the spherical media type RS 11 G, two workpiece positions $x_w = 5 \text{ mm}$ and $x_w = 15 \text{ mm}$ could be identified, where increased roughness reductions of up to $\Delta Ra = 80\%$ were present. The distances of the positions of increased roughness reduction to the adapters were 5 mm each, which corresponds approximately to the radius of the spherical media. Therefore, it can be concluded that the machining of the surface predominantly occurred by a contact constellation in which the media were in contact with the adapters when sliding or rolling over the surface, Figure 10b. Between the two positions of increased roughness reduction, an average roughness reduction of $\Delta Ra = 33\%$ could be observed. This also applied to the workpiece positions $x_w < 5 \text{ mm}$ and $x_w > 15 \text{ mm}$, where an average roughness reduction of $\Delta Ra = 35\%$ was present. Due to geometrical restrictions, no accessibility and thus no machining at these positions was possible with this media type; therefore, it can be concluded that machining at these positions was performed only by abraded particles of the media. For the cylindrical media type RS 07/15 SZ, three workpiece positions $x_w = 4 \text{ mm}$, $x_w = 10 \text{ mm}$, and $x_w = 17 \text{ mm}$ with an increased roughness reduction of up to $\Delta Ra = 70\%$ could be observed. Considering the radius of the cylindrical media, it can be concluded that machining predominantly occurred by a contact constellation in which two pieces of media slide over the surface side by side in the direction of their longitudinal axis, with one piece of media in contact with the adapter, Figure 10b. Between the three positions of

the increased roughness reduction, an average roughness reduction of $\Delta Ra = 41\%$ could be observed. At workpiece positions $x_w = 1$ mm and $x_w = 19$ mm, a low average roughness reduction of $\Delta Ra = 20\%$ could be observed due to a limited access of the media to the surface close to the adapters. For the prismatic media type RS 10/15 S, a more uniform roughness reduction ΔRa could be observed than for the other media types, especially between the workpiece positions $x_w = 5$ mm and $x_w = 15$ mm, where the average roughness reduction was $\Delta Ra = 57\%$. From these positions, the roughness reduction ΔRa slightly increased towards the central workpiece position $x_w = 10$ mm. The highest roughness reductions of up to $\Delta Ra = 71\%$ were present at the workpiece positions $x_w = 2$ mm and $x_w = 18$ mm. This might result from a contact constellation in which a piece of media was in contact with the workpiece with its edge while it was supported by the adapter and another piece of media, which was in contact with the workpiece with its surface, Figure 10b. Again, due to the limited access of the media to the surface close to the adapters, a low average roughness reduction of $\Delta Ra = 38\%$ could be observed at the workpiece positions $x_w = 1$ mm and $x_w = 19$ mm. It should also be mentioned that despite the cylindrical media type RS 07/15 SZ, the influence of the rotational speed n_d seemed to be less significant for the machining of workpiece variant B than for workpiece variant A.

For the spherical media type RS 11 G, the two workpiece positions $x_w = 5$ mm and $x_w = 15$ mm of increased roughness reduction ΔRa were predicted with high accuracy, Figure 10c. The predicted roughness reductions of $\Delta Ra = 75\%$ at these two positions matched the results from experiments. Between the two positions of increased roughness reduction, a roughness reduction of $\Delta Ra = 38\%$ was predicted, which was in agreement with experimental results. Contrarily to the finishing experiments, abraded particles of the media were not present in the DEM simulations. Therefore, the finishing results at the workpiece positions $x_w < 5$ mm and $x_w > 15$ mm could not be reflected by the prediction model as no contacts between the media and the workpiece occurred due to geometrical restrictions. Consequently, a roughness reduction of $\Delta Ra = 0\%$ was predicted at these positions. For the cylindrical media type RS 07/15 SZ, the three workpiece positions $x_w = 4$ mm, $x_w = 10$ mm, and $x_w = 17$ mm with an increased roughness reduction ΔRa were predicted with a high accuracy, Figure 10c. At these three positions, an average roughness reduction of $\Delta Ra = 73\%$ was predicted, which was in agreement with the experimental results. Between the positions of increased roughness reduction ΔRa and at the positions close to the adapters, an average roughness reduction of $\Delta Ra = 61\%$ and $\Delta Ra = 55\%$ was predicted, respectively. Although this matched the experimental results qualitatively, the roughness reductions ΔRa at these workpiece positions x_m were overestimated by the prediction model. Furthermore, the effect of the rotation speed n_d was less observable in the predicted results than in the experimental results. As observed in the experimental results, the most uniform roughness reduction ΔRa was predicted for the prismatic media type RS 10/15 S, Figure 10c. Between the workpiece positions $x_w = 5$ mm and $x_w = 15$ mm, an average roughness reduction of $\Delta Ra = 66\%$ was predicted, which was slightly higher compared to the experimental results. The highest roughness reductions of up to $\Delta Ra = 80\%$ occurred close to the adapters at the workpiece positions $x_w = 1$ mm and $x_w = 19$ mm. As derived from the experimental results, this resulted from a contact constellation in which a piece of media was in contact with the workpiece with its edge while it was supported by the adapter and another piece of media, Figure 10b. However, the limited access of the media to the workpiece positions $x_w = 1$ mm and $x_w = 19$ mm resulting in a low roughness reduction ΔRa in the experiments could not be reflected by the predictions.

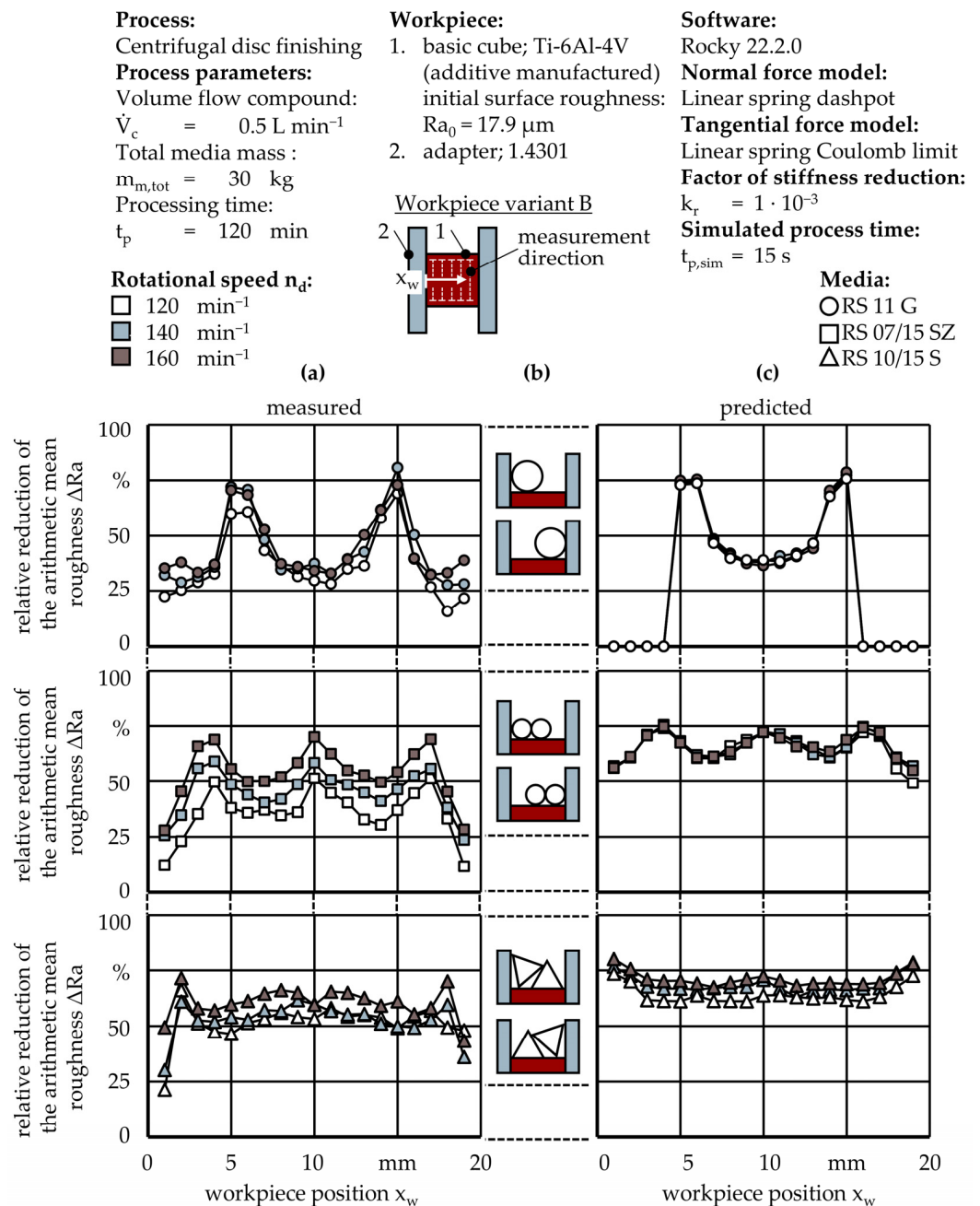


Figure 10. Workpiece variant B: (a) results of finishing experiments; (b) predominant contact constellations; (c) predicted finishing results.

4. Discussion

By using the DEM with force–displacement laws derived by Cundall and Strack [12] and a series of experiments to determine a set of contact parameters, a simulation of the centrifugal disc finishing was devised. A force-based validation showed that the simulated results deviated by 20% from the experimental results on average, which is considered a reasonable accuracy considering previous approaches of modeling mass finishing processes with the DEM [13,26]. The simulated results were consistent with the experimental results regarding the influence of the rotational speed n_d as well as the influence of the media type on the contact normal forces $F_{c,n}$. Consequently, it can be concluded that the presented model assumptions, Sections 2.4.1 and 2.4.2, as well as the conducted series of experiments to determine the contact parameters are valid. Especially, the transfer of the contact parameters determined for a certain media type to another media type of the same material,

but of a different shape, might be useful to simplify the procedure of contact parameter determination. In addition, it was shown that reducing the contact stiffness is a useful method to reduce the computational time t_{comp} of DEM simulations, while the effects of influential factors remain observable. Considering only the contact normal forces $F_{c,n}$ were found to be insufficient when predicting the finishing results, as this neglects the effect of the media shape. Thus, the overall contact intensity I_c transferred from the media to the surface of the workpiece was introduced. Although this characteristic does not include the tangential contact velocity $v_{c,t}$ of the media in contact with the workpiece, which is known to be related to material removal in mass finishing [43], it shows a clear correlation to the roughness reduction obtained in the finishing experiments, Figure 9b. It is emphasized that the contact intensity I_c is to be considered as a general characteristic of the machining intensity and is not used to describe material removal mechanisms. By empirically fitting the roughness reduction ΔRa to the contact intensity I_c using a power law approach, a prediction model was derived considering the constraint that a contact intensity of $I_c = 0 \text{ W m}^{-2}$ would not result in any machining, Equation (10). The prediction model was used to predict the finishing results of a workpiece with a limited accessibility to its surface. As expected, local differences in the finishing results depending on the type of media were observable. For the spherical media type RS 11 G and the cylindrical media type RS 07/15 G, the characteristics of the local roughness reduction ΔRa were reflected by the prediction model, which led to the conclusion that predominant contact constellations could be successfully modeled using the DEM. However, the low roughness reductions observed in the experimental results were overestimated by the prediction model. This can be attributed to the fact that the prediction model was derived from data only ranging from contact intensities of $I_c = 1.9 \text{ W m}^{-2}$ to $I_c = 9.5 \text{ W m}^{-2}$ and roughness reductions of $\Delta Ra = 67\%$ to $\Delta Ra = 88\%$, Figure 9b. Using the prediction model outside this range of data, which is the case when finishing the workpiece with limited accessibility, leads to inaccuracies in predictions. Consequently, future work should extend the range of the validity of the prediction model. The prediction model predicted a uniform roughness reduction for the prismatic media type RS 10/15 S, which was in agreement with the finishing results. However, the limited access of the media to the surface near to the adapters could not be reflected, which requires further investigation.

5. Conclusions

In this study, it was shown that the complex relationship between the type of media, the accessibility to the surface, and the achievable finishing results can be modeled using the DEM. Therefore, when finishing complex-shaped workpieces, DEM simulations could be used in the process design to select suitable media, which usually requires an extensive know how about mass finishing processes. Future work will concern the investigation of local material removal, as this is of particular importance when it comes to the shape accuracy of workpieces machined by centrifugal disc finishing. The main findings of the study can be summarized as follows:

- The high as-built roughness of additive manufactured workpieces was reduced from $Ra_0 = 17.9 \text{ }\mu\text{m}$ to $Ra = 2.1 \text{ }\mu\text{m}$ ($\Delta Ra = 88.3\%$) in a process time of $t_p = 120 \text{ min}$ using centrifugal disc finishing.
- A simulation of the centrifugal disc finishing based on the DEM was devised. Simulated contact normal forces $F_{c,n}$ deviated from the experimental results by 20% on average.
- The contacts intensity I_c obtained by DEM simulations correlated with the roughness reduction of the additive manufactured workpieces for different media types and rotational speeds n_d .
- A limited accessibility to the surface led to local differences in the roughness reduction ΔRa , which depended on the media type.

- By empirically linking the simulated contacts intensity I_c with the roughness reduction ΔRa , the local differences in the roughness reduction ΔRa could be predicted qualitatively.

Author Contributions: Conceptualization, M.K. and E.U.; methodology, E.U.; software, M.K.; validation, M.K.; formal analysis, M.K.; investigation, M.K.; resources, M.K.; data curation, M.K.; writing—original draft preparation, M.K.; writing—review and editing, E.U.; visualization, M.K.; supervision, E.U.; project administration, E.U.; funding acquisition, E.U. All authors have read and agreed to the published version of the manuscript.

Funding: This research was funded by the German Research Foundation (DFG) (Bonn, Germany) within the scope of the project “Nachbearbeitung additiv gefertigter Werkstücke mittels Fliehkraftgleitschleifen”, project number 460895790.

Institutional Review Board Statement: Not applicable.

Informed Consent Statement: Not applicable.

Data Availability Statement: Not applicable.

Acknowledgments: The authors kindly thank Cadfem GmbH, Grafing (Munich), Germany, for providing the software Rocky DEM, and Rösler Oberflächentechnik GmbH, Untermerzbach, Germany, for providing the abrasive media.

Conflicts of Interest: The authors declare no conflict of interest.

References

1. Gillespie, L.K. *Mass Finishing Handbook*, 1st ed.; Industrial Press: La Vergne, TN, USA, 2006.
2. Uhlmann, E.; Eulitz, A.; Seiffert, K.; Kersting, R.; Schenk, S. Finishing of additive manufactured titanium parts—Potentials of centrifugal disc finishing. *Werkstattstech. Online* **2019**, *109*, 402–406. [[CrossRef](#)]
3. Kahlin, M.; Ansell, H.; Basu, D.; Kerwin, A.; Newton, L.; Smith, B.; Moverare, J.J. Improved fatigue strength of additively manufactured Ti6Al4V by surface post processing. *Int. J. Fatigue* **2020**, *134*, 105497. [[CrossRef](#)]
4. Kahlin, M.; Ansell, H.; Kerwin, A.; Smith, B.; Moverare, J.J. Variable amplitude loading of additively manufactured Ti6Al4V subjected to surface post processes. *Int. J. Fatigue* **2021**, *142*, 105945. [[CrossRef](#)]
5. Gerlitzky, G. Einfluss des Post-Processings auf Laserstrahlgeschmolzene Bauteile am Beispiel von β -Titanlegierungen. Ph.D. Thesis, Technische Universität Berlin, Berlin, Germany, 2021.
6. Güneşsu, E.; Yılmaz, M.S.; Taşcıoğlu, E.; Sharif, S.; Kaynak, Y. Effect of Drag Finish Post-processing on Surface Integrity and Wear Behavior of Ti-6Al-4V Fabricated by Laser Powder Bed Fusion Additive Manufacturing. *J. Mater. Eng. Perform.* **2022**, *117*, 371. [[CrossRef](#)]
7. Kaynak, Y.; Tascioglu, E. Post-processing effects on the surface characteristics of Inconel 718 alloy fabricated by selective laser melting additive manufacturing. *Prog. Addit. Manuf.* **2020**, *5*, 221–234. [[CrossRef](#)]
8. Zanger, F.; Kacaras, A.; Neuenfeldt, P.; Schulze, V. Optimization of the stream finishing process for mechanical surface treatment by numerical and experimental process analysis. *CIRP Annals* **2019**, *68*, 373–376. [[CrossRef](#)]
9. Malkorra, I.; Souli, H.; Salvatore, F. Numerical modelling of the drag finishing process at a macroscopic scale to optimize surface roughness improvement on additively manufactured (SLM) Inconel 718 parts. *Procedia CIRP* **2022**, *108*, 648–653. [[CrossRef](#)]
10. Malkorra, I.; Souli, H.; Claudin, C.; Salvatore, F.; Arrazola, P.; Rech, J.; Seux, H.; Mathis, A.; Rolet, J. Identification of interaction mechanisms during drag finishing by means of an original macroscopic numerical model. *Int. J. Mach. Tools Manuf.* **2021**, *168*, 103779. [[CrossRef](#)]
11. Eulitz, A. Einsatzverhalten Keramisch Gebundener Gleitschleifkörper. Ph.D. Thesis, Technische Universität Berlin, Berlin, Germany, 2021.
12. Cundall, P.A.; Strack, O.D.L. A discrete numerical model for granular assemblies. *Géotechnique* **1979**, *29*, 47–65. [[CrossRef](#)]
13. Uhlmann, E.; Eulitz, A.; Dethlefs, A. Discrete Element Modelling of Drag Finishing. *Procedia CIRP* **2015**, *31*, 369–374. [[CrossRef](#)]
14. Naeini, S.E.; Spelt, J.K. Two-dimensional discrete element modeling of a spherical steel media in a vibrating bed. *Powder Technol.* **2009**, *195*, 83–90. [[CrossRef](#)]
15. Naeini, S.E.; Spelt, J.K. Development of single-cell bulk circulation in granular media in a vibrating bed. *Powder Technol.* **2011**, *211*, 176–186. [[CrossRef](#)]
16. Hashemnia, K.; Mohajerani, A.; Spelt, J.K. Development of a laser displacement probe to measure particle impact velocities in vibrationally fluidized granular flows. *Powder Technol.* **2013**, *235*, 940–952. [[CrossRef](#)]
17. Hashemnia, K.; Spelt, J.K. Particle impact velocities in a vibrationally fluidized granular flow: Measurements and discrete element predictions. *Chem. Eng. Sci.* **2014**, *109*, 123–135. [[CrossRef](#)]

18. Da Silva Maciel, L.; Spelt, J.K. Influence of process parameters on average particle speeds in a vibratory finisher. *Granul. Matter* **2018**, *20*, 65. [[CrossRef](#)]
19. Da Silva Maciel, L.; Spelt, J.K. Comparison of DEM predictions and measured wall-media contact forces and work in a vibratory finisher. *Powder Technol.* **2020**, *366*, 434–447. [[CrossRef](#)]
20. Da Silva Maciel, L.; Spelt, J.K. Measurements of wall-media contact forces and work in a vibratory finisher. *Powder Technol.* **2020**, *360*, 911–920. [[CrossRef](#)]
21. Hashemnia, K.; Pourandi, S. Study the effect of vibration frequency and amplitude on the quality of fluidization of a vibrated granular flow using discrete element method. *Powder Technol.* **2018**, *327*, 335–345. [[CrossRef](#)]
22. Kang, Y.S.; Hashimoto, F.; Johnson, S.P.; Rhodes, J.P. Discrete element modeling of 3D media motion in vibratory finishing process. *CIRP Annals* **2017**, *66*, 313–316. [[CrossRef](#)]
23. Wang, X.; Yang, S.; Li, W.; Wang, Y. Vibratory finishing co-simulation based on ADAMS-EDEM with experimental validation. *J. Adv. Manuf. Technol.* **2018**, *96*, 1175–1185. [[CrossRef](#)]
24. Makiuchi, Y.; Hashimoto, F.; Beaucamp, A. Model of material removal in vibratory finishing, based on Preston's law and discrete element method. *CIRP Annals* **2019**, *68*, 365–368. [[CrossRef](#)]
25. Salvatore, F.; Grange, F.; Kaminski, R.; Claudin, C.; Kermouche, G.; Rech, J.; Texier, A. Experimental and Numerical Study of Media Action During Tribofinishing in the Case of SLM Titanium Parts. *Procedia CIRP* **2017**, *58*, 451–456. [[CrossRef](#)]
26. Uhlmann, E.; Kopp, M. Measurement and Modeling of Contact Forces during Robot-guided Drag Finishing. *Procedia CIRP* **2021**, *102*, 518–523. [[CrossRef](#)]
27. Kopp, M.; Uhlmann, E. Potential of Robot-Guided Centrifugal Disc Finishing. In *Production at the Leading Edge of Technology*; Behrens, B.-A., Brosius, A., Drossel, W.-G., Hintze, W., Ihlenfeldt, S., Nyhuis, P., Eds.; Springer International Publishing: Cham, Switzerland, 2022; pp. 283–291. [[CrossRef](#)]
28. Uhlmann, E.; Kopp, M.; Fürstenau, J.-P. Modelling of media wear in centrifugal disc finishing. *Werkstattstech. Online* **2022**, *112*, 458–464. [[CrossRef](#)]
29. Uhlmann, E.; Fürstenau, J.-P.; Kuche, Y.; Yabroudi, S.; Polte, J.; Polte, M. Modeling of the wet immersed tumbling process with the Discrete Element Method (DEM). *Procedia CIRP* **2021**, *102*, 1–6. [[CrossRef](#)]
30. Cariapa, V.; Park, H.; Kim, J.; Cheng, C.; Evaristo, A. Development of a metal removal model using spherical ceramic media in a centrifugal disk mass finishing machine. *Adv. Manuf. Technol.* **2008**, *39*, 92–106. [[CrossRef](#)]
31. Wan, S.; Sato, T.; Hartawan, A. Vibratory Finishing of Immobilized Cylinders. *Adv. Mat. Res.* **2012**, *565*, 278–283. [[CrossRef](#)]
32. Wan, S. A Framework for the Analysis of Mass Finishing Processes. *Adv. Mat. Res.* **2012**, *565*, 284–289. [[CrossRef](#)]
33. Ten, J.S.; Wan, S. Benchmarking study on continuum-based granular flow dynamics models for simulating the drag finishing process on a CFD framework. *Int. J. Abras. Technol.* **2014**, *6*, 214–225. [[CrossRef](#)]
34. Mullany, B.; Shahinian, H.; Navare, J.; Azimi, F.; Fleischhauer, E.; Tkacik, P.; Keanini, R. The application of computational fluid dynamics to vibratory finishing processes. *CIRP Annals* **2017**, *66*, 309–312. [[CrossRef](#)]
35. Kopp, M.; Uhlmann, E.; Kneider, C. Experimental investigations of the workpiece-media-interaction and the surface topography formation in centrifugal disc finishing. *Procedia CIRP* **2022**, *115*, 24–29. [[CrossRef](#)]
36. *DIN EN ISO 4287*; Geometrische Produktspezifikation (GPS)—Oberflächenbeschaffenheit: Tastschnittverfahren—Benennungen, Definitionen und Kenngrößen der Oberflächenbeschaffenheit. Beuth: Berlin, Germany, 2010.
37. *DIN EN ISO 4288*; Geometrische Produktspezifikationen (GPS)—Oberflächenbeschaffenheit: Tastschnittverfahren Regeln und Verfahren für die Beurteilung der Oberflächenbeschaffenheit. Beuth: Berlin, Germany, 1998.
38. Malone, K.F.; Xu, B.H. Determination of contact parameters for discrete element method simulations of granular systems. *Particuology* **2008**, *6*, 521–528. [[CrossRef](#)]
39. Schwager, T.; Pöschel, T. Coefficient of restitution and linear-dashpot model revisited. *Granul. Matter* **2007**, *9*, 465–469. [[CrossRef](#)]
40. Tsuji, Y.; Kawaguchi, T.; Tanaka, T. Discrete particle simulation of two-dimensional fluidized bed. *Powder Technol.* **1993**, *77*, 79–87. [[CrossRef](#)]
41. González-Montellano, C.; Fuentes, J.M.; Ayuga-Téllez, E.; Ayuga, F. Determination of the mechanical properties of maize grains and olives required for use in DEM simulations. *J. Food Eng.* **2012**, *111*, 553–562. [[CrossRef](#)]
42. Lommen, S.; Schott, D.; Lodewijks, G. DEM speedup: Stiffness effects on behavior of bulk material. *Particuology* **2014**, *12*, 107–112. [[CrossRef](#)]
43. Hashimoto, F.; Johnson, S.P.; Chaudhari, R.G. Modeling of material removal mechanism in vibratory finishing process. *CIRP Annals* **2016**, *65*, 325–328. [[CrossRef](#)]